eMethods

Plasma P-Tau181 and P-Tau217 Processing and Assay Development

Blood samples were obtained by venipuncture in ethylenediaminetetraacetic acid (EDTA) tubes for plasma, following the ADNI protocol.[1] Within 60 minutes, the samples were centrifuged at 3000 rpm at room temperature, aliquoted and stored at -80°C. The pTau assays were designed to measure pTau in plasma (either P-Tau217 or P-Tau181) and optimized to measure disease-related differences through the selection of monoclonal antibodies used in the assays. Detector antibodies were conjugated with NHS-PEG4-Biotin (Thermo Scientific, catalog number: 21329) or MSD GOLD SULFO-TAG NHS-Ester (MSD, catalog number: R91AO-1) according to the manufacturer's protocol. Selection of the monoclonal antibody pairs provided a unique combination of sensitivity and selectivity for the tau forms in plasma that are different between HC and AD subjects. Each assay was calibrated using a synthetic pTau peptide specific for the epitope of the assay coupled to the tau peptide corresponding to the 4G10-E2 epitope with a PEG12 linker. The fully synthetic peptide-based calibrators were verified for purity >95% by HPLC and identity by mass spectrometry.

The plasma samples were thawed on wet ice, briefly vortexed, and diluted 1:2 in sample diluent with the addition of Heterophilic Blocking Reagent 1 to a concentration of 200 ug/mL (Scantibodies Inc, catalog number: 3KC533). In order the run the assay, MSD small-spot streptavidin (MSD, L45SA) coated plates were blocked for 1 hour at room temperature with 200 uL of 3% BSA and 2% PEG in PBS with 650 rpm shaking on a plate shaker. The plates were then washed three times with 200 uL of wash buffer (PBS + 0.05% Tween 20) and 25 uL of biotinylated capture antibody was added and incubated for 1 hour at room temperature with 650 rpm shaking on a plate shaker. The plates were again washed three times with 200 uL of wash buffer and 50 uL of diluted calibrator or sample was added to the plate and incubated for 2 hours at room temperature with 650 rpm shaking on a plate shaker. The plates were then washed three times with 200 uL of wash buffer and 25 uL of SULFO-tagged 4G10-E2 detection antibody was added and incubated for 1 hour at room temperature with 650 rpm shaking on a plate shaker. The plates were washed a final time with 200 uL of wash buffer and 150 uL of 2X MSD Read Buffer T with Surfactant (MSD, R92TC) was added to each plate and read on the MSD SQ120 within 10 minutes of read buffer addition. Results were calculated by the MSD software using a 4PL, 1/y2 weight of the standard curve for interpolation.

P-tau217 and P-tau181 Assay Optimization for Comparability

Assay Conditions

	P-Tau217	**P-Tau181**
Block Buffer	PBS + 3% BSA +2% PEG	PBS + 3% BSA +2% PEG
Capture Buffer	PBS + 0.1% BSA + 0.05% Tween 20 + 2% PEG	PBS + 0.1% BSA + 0.05% Tween 20 + 2% PEG
Calibrator Diluent	Low Salt Buffer	Low Salt Buffer
Sample Diluent	Low Salt Buffer + 200 ug/mL HBR1	Low Salt Buffer + 200 ug/mL HBR1
Detection Buffer	Low Salt Buffer	Low Salt Buffer
Read Buffer	2x MSD Read Buffer T	2x MSD Read Buffer T
Capture Antibody	IBA493	AT270
Capture Antibody Conc.	0.5 ug/mL	1 ug/mL
Detection Antibody	4G10-E2	4G10-E2
Detection Antibody Conc	0.02 ug/mL	0.02 ug/mL

Calibrator	Synthetic P-Tau217 Peptide	Synthetic P-Tau181 Peptide

Between two runs of samples obtained from UCSF in collaboration on P-Tau217 and P-Tau181, both assays went through a series of improvements to address assay robustness over time, buffer optimizations, and condition alignment as much as possible in order to facilitate co-analysis of both P-Tau217 and P-Tau181 simultaneously. To accomplish this, the following changes were implemented:

1. DPBS was replaced with PBS in order to maintain control over, and increase, the buffering capacity of the buffers since DPBS has low buffering capacity.
2. 2% polyethylene glycol (PEG) was added to block buffer, capture buffer, and is present in the low salt buffer. This addition is intended to reduce non-specific binding at all stages and improve the signal to noise ratio of the samples.
3. MSD Diluent 35 was replaced by low salt buffer for both performance improvements and in order to have a fully defined buffer and non-proprietary buffer for consistency.
4. The LRL detection antibody was replaced with 4G10-E2 in the P-Tau181 assay due to the identification of long-term storage and stability issues that were causing a performance concern, which was remedied by implementation of the 4G10-E2 total tau antibody replacement.
5. Synthetic peptides replaced an *in vitro* phosphorylated full-length tau protein for consistency purposes. Historically, pTau was generated via an enzymatic reaction with GSK-3beta, however this approach required significant characterization and the approach was very difficult to maintain lot to lot consistency in manufacturing of the calibrator. By using a synthetic peptide, the control over the assay is vastly improved. Each calibrator is characterized using mass spectrometry to confirm sequence identity and HPLC to confirm purity. The long-term stability and performance properties of these new calibrators are being assessed.

PET Acquisition and Processing

Participants were scanned on one of three scanners: a Siemens Biograph 6 PET/CT scanner or ECAT PET scanner at the Lawrence Berkeley National Laboratory, or a GE Discovery STE/VCT PET-CT at UCSF Imaging Center at China Basin. Attenuation correction was performed using either an emission scan (PET scanners) or low-dose CT scan (PET-CT scans). All scanners were certified priori to data acquisition following ADNI procedures (http://adni.loni.usc.edu/methods/). PET acquisition and processing procedures are also detailed elsewhere[2].

Amyloid-PET was performed with [11C]Pittsburgh Compound B (PIB, injected dose: ~15mCi; N=101) or [18F]Florbetapir (FBP; injected dose: ~10mCi; N=30). Tau-PET was performed using [18F]Flortaucipir (FTP; injected dose: ~10mCi; N=78). A dynamic PIB-PET scan was acquired for 90min immediately after intravenous PIB injection. FBP-PET acquisition included four 5-min frames between 50-70min post injection. FTP-PET scan acquisition varied in their timing, although always including the 80–100min post injection window. FTP and PIB scans were reconstructed using an ordered subset expectation maximum algorithm with weighted attenuation and were smoothed using a 4 mm Gaussian kernel with scatter correction (calculated image resolution 6.5 × 6.5 × 7.25 mm using Hoffman phantom). FBP scan reconstruction followed ADNI protocols (http://adni.loni.usc.edu/methods/).

Reconstructed PET frames were realigned for motion correction and coregistered with reslicing to participants' T1-weighted MRIs. Mean count images were converted into voxel-wise Standardized Uptake Value Ratio (SUVR) images (FBP-PET and PIB-PET, 50-70min; FTP-PET, 80-100min) using tracer specific reference regions defined using Freesurfer-derived MRI parcellation and the SUIT atlas, as previously defined[3]. Tracer specific reference regions were whole cerebellum for FBP, cerebellar gray matter for PIB, and inferior cerebellar gray matter for FTP. PET images were warped to MNI space with the MRI-based transformations. Finally, PET images were differentially smoothed to obtain about the same final resolution (i.e., about 8 mm^3 isotropic).

FBP-PET and PIB-PET SUVR images were centrally read as positive or negative at UCSF based on visual assessment[4]. SUVRs were then converted to Centiloids (CLs) scale to harmonize data across the two tracers using the following conversions: PiB CL= (SUVR × 95.57) – 94.75[5]; Florbetapir CL = (SUVR x 196.9) – 196.03. FBP-PET SUVR conversion to CLs followed ADNI procedures (http://adni.loni.usc.edu/methods/pet-analysis-method/pet-analysis/). A value of 100 CLs corresponds with the average degree of amyloid deposition observed in patients diagnosed with Alzheimer's disease dementia[6]. To quantify Flortaucipir binding, we extracted SUVR values from the whole cortex. An overall cortical SUVR was calculated with FTP-PET positivity defined as SUVR>1.22[7].

eTables and eFigures

	Suggestive of CTE[a]	Possible CTE	Probable CTE	Sig.
N	6	5	7	-
Age	54.8 (47.5-64.6)	68.1 (61.7-73.3)	69.4 (64.4-79.0)	.09
P-tau181 (pg/mL)	1.06 (0.74-1.98)	0.82 (0.55-1.54)	1.34 (0.59-1.77)	.67
P-tau217 (pg/mL)	0.18 (0.14-0.34)	0.18 (0.14-0.44)	0.34 (0.09-0.42)	.96
Aβ-PET, Centiloids[b]	-4.9 (-10.3-48.4)	54.3 (5.8-79.7)	10.1 (3.0-29.2)	.39
Aβ status, + / - [b]	2 / 4	4 / 1	4 / 3	-

[a] One patient with TES met 2014 research diagnostic criteria but not the 2021 update. This patient was included in the "Suggestive of CTE" group.

[b] Aβ-PET was available for all but one patient with TES (classified as "Suggestive of CTE"), whose Aβ status was determined to be negative based on absence of diffuse or neuritic Aβ plaques at autopsy (Thal phase 0). Centiloid values could be calculated for 16 of the 17 patients with TES and an Aβ-PET scan due to lack of corresponding structural MRI in one participant.

eTable 1: Descriptive data and plasma P-tau concentrations across levels of diagnostic certainty in patients with TES. Values are presented as median (interquartile range). Statistical significance of group comparisons was based on analysis of variance with log-transformed dependent variables. The comparisons of plasma P-tau concentrations and Aβ burden (Centiloids) controlled for age.

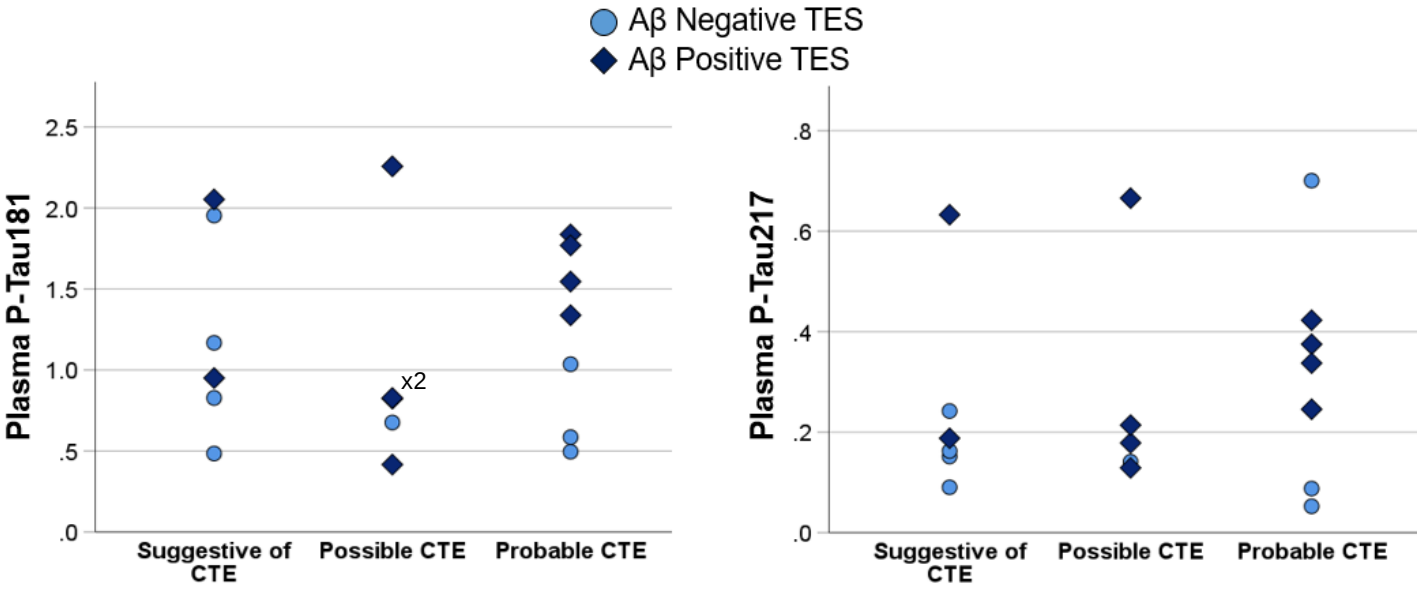

eFigure 1: Visual depiction of plasma P-tau181 and P-tau217 concentrations stratified by levels of diagnostic certainty in patients with TES. Two patients with "Possible CTE" had nearly identical plasma P-tau181 concentrations (0.82 and 0.83 pg/mL) so those data points overlap in the figure (designated by "x2" notation).

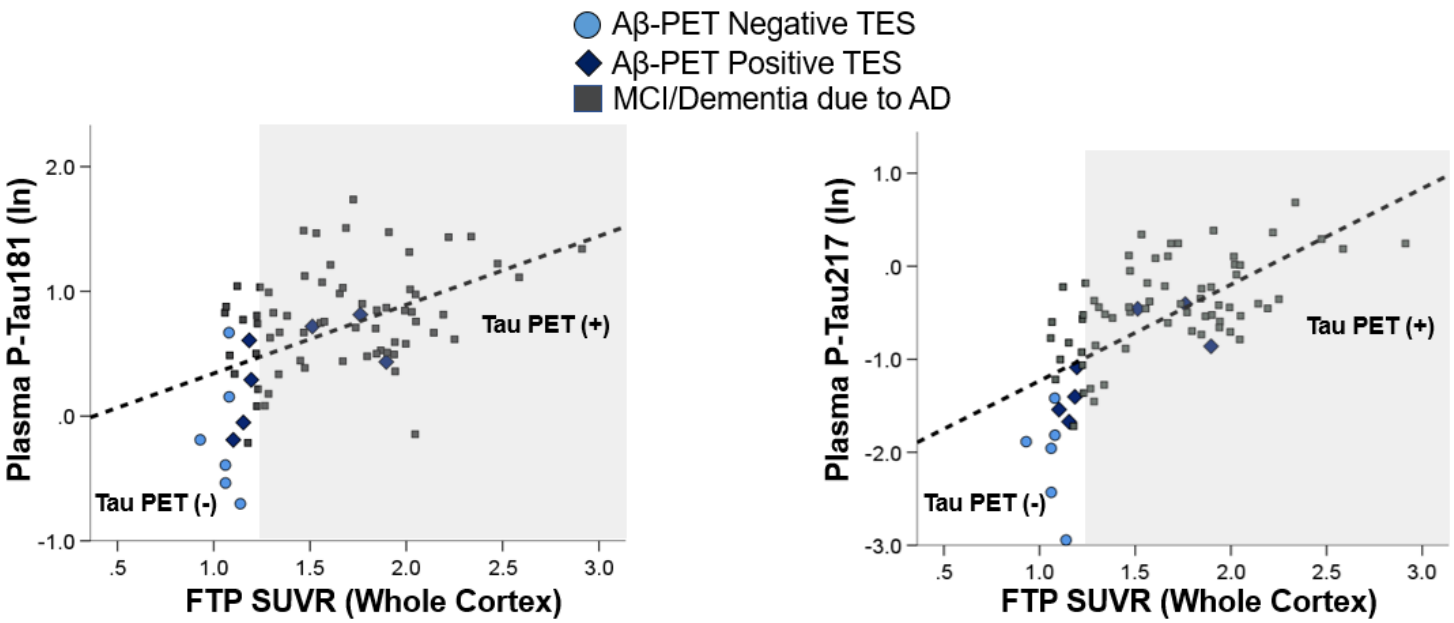

eFigure 2: Plasma P-Tau181 and P-Tau217 are not associated with flortaucipir (FTP) PET signal (whole cortex average) in Aβ-PET negative TES patients. However, similar to patients with MCI/dementia due to AD and no known prior head trauma, Aβ-PET positive TES patients showed a positive association between plasma P-Tau181 and P-Tau217 with cortical FTP-PET signal. The grey shaded area represents the quantitative threshold for FTP-PET positivity in the whole cortex (SUVR>1.22). Of note, when examining a temporal meta-region of interest including regions most vulnerable to AD pathology, all MCI/dementia due to AD patients and an additional 3 Aβ-PET positive TES patients exceeded the region-specific quantitative threshold for FTP-PET positivity consistent with AD (data not shown).

Patient	Age at Death	Neuropathologic Findings	CTE Classification	Qualitative Description of Tau Pathology
A	72	Primary: CTE Contributing: Limbic-predominant TDP-43 proteinopathy with focal hippocampal sclerosis (left CA1), vascular brain injury with old microinfarct (left subiculum) Incidental: Limbic AGD, ARTAG, mild arteriolosclerosis	High CTE (McKee Stage IV)	Perivascular lesions characterized by the presence of numerous tau-immunoreactive astrocytes and occasional neuronal cytoplasmic inclusions/neurofibrillary tangles were observed in the frontal pole, anterior orbital gyrus, anterior cingulate cortex, middle frontal gyrus, inferior frontal gyrus, middle insula, amygdala, hypothalamus, superior frontal sulcus, dentate gyrus, superior and middle temporal gyrus, angular gyrus, and posterior white matter tracts of the lumbar cord. Clusters of neuronal and astrocytic cytoplasmic inclusions were seen at the depth of sulci in the middle frontal gyrus, inferior frontal gyrus, middle insula, superior frontal sulcus, superior and middle temporal gyrus, postcentral cortex, and angular gyrus. Severity and topographic distribution of these findings was consistent with Stage IV CTE.
B	59	Primary: FTLD-TDP43 (Type B) with motor neuron disease Incidental: CTE, limbic AGD, ARTAG, ATAC, mild arteriolosclerosis	High CTE (McKee Stage IV)	Numerous neurofibrillary tangles were observed in multiple cortical layers in the frontal pole, anterior orbital gyrus, anterior and subgenual cingulate gyrus, middle and inferior frontal gyrus, premotor cortex, superior, middle and inferior temporal gyri, insula, and angular gyrus, as well as in the ventral striatum and amygdala, dentate nucleus, substantia nigra, tectum and periaqueductal grey, and locus coeruleus. Abundant thorny-shaped-like astrocytes and oligodendroglial coiled bodies were seen in the correspondent subcortical white matter. Numerous astrocytes with diffuse or granule tau-immunoreactive cytoplasmic inclusions and a few tau-immunoreactive neurons were observed at the depth of sulci and/or perivascular regions in the frontal pole, anterior orbital gyrus, anterior and subgenual cingulate gyrus, middle and inferior frontal gyrus, insular cortex, entorhinal cortex, premotor cortex, superior, middle and inferior temporal gyri, and angular gyrus. Tau-immunoreactive astrocytes were noted in the subependymal layers of frontal pole, premotor cortex, superior and middle temporal gyri, and angular gyrus, as well as in the periaqueductal gray. ATAC were found in the subgenual cingulate gyrus. Severity and topographic distribution of these findings was consistent with Stage IV CTE.
C*	81	Primary: Alzheimer's disease (low-to-moderate ADNC) Contributing: Limbic-predominant TDP-43 proteinopathy Incidental: Limbic AGD, ARTAG, CTE, Lewy body disease (brainstem), CAA	Low CTE (McKee Stage I)	Numerous tau-immunoreactive neurons were concentrated in the hippocampus, entorhinal cortex, amygdala, temporal cortex and several brainstem nuclei including the substantia nigra, locus coeruleus, dorsal raphe nucleus, superior colliculus, periaqueductal grey, cranial nerve III complex, nucleus ambiguous, and dorsal motor nucleus of the vagus. In addition to the tauopathy in neurons, there were scattered astrocytes and dystrophic neurites with tau-positive protein aggregates. The morphological features of the tau aggregates were quite broad, ranging from flame-shaped neurofibrillary tangles in cortical neurons to globus neurofibrillary tangles, more common in the brainstem, to diffuse cytoplasmic aggregates. Rare involvement of CTE-consistent tau pathology was identified in the frontal cortex at one sulcus, with astrogliosis and microgliosis throughout the frontal and temporal lobes, especially at subpial, grey-white junction, and subcortical white matter distribution. Severity and topographic distribution of these findings was consistent with Stage I CTE.

D	79	Primary: Alzheimer's Disease (High ADNC; A3B3C3) Contributing: limbic TDP-43 proteinopathy with bilateral hippocampal sclerosis Incidental: CTE, chronic lymphocytic leukemia, limbic AGD, ATAC, mild arteriolosclerosis	Low CTE (McKee Stage I)	Several clusters of tau-immunoreactive neurons and/or astrocytes were observed at the depth of sulci or in perivascular spaces in the middle frontal gyrus. Tau-immunoreactive neurons and/or astrocytes were also observed in entorhinal cortex and postcentral gyrus (without predilection for perivascular spaces or sulcal depths), together with moderate amount of neurofibrillary tangles and bushy astrocytes throughout the cortical layers. Numerous neurofibrillary tangles were seen in the substantia nigra. Sparse neurofibrillary tangles and bushy astrocytes were seen in the frontal pole cortex, anterior cingulate gyrus, premotor cortex, thalamus, and periaqueductal gray. Abundant ATAC were seen in the peri-amygdaloid region and periaqueductal grey. Severity and topographic distribution of these findings was consistent with Stage I CTE.

*****Determination of primary, contributing, and incidental neuropathological findings for this patient was limited by incomplete clinical information

eTable 2: Additional neuropathological details for 4 patients with TES who went to autopsy and were diagnosed with CTE. Characterization of CTE pathology is indicated using both the recently proposed "High" vs. "Low" schema (Bieniek et al., 2021) and the McKee staging criteria (McKee et al., 2013). Tau pathology was described qualitatively by the reviewing neuropathologist. "Primary" neuropathological diagnosis is defined as the most developed neuropathological entity, as ascertained through neuropathological evaluation. The primary diagnosis(es) are thought to explain the majority of the clinical cognitive and behavioral phenotype manifested by the patient on the basis of the severity and regional distribution of the neuropathological findings. "Contributing" neuropathological diagnoses are defined as coexistent neuropathological entities that are sufficiently developed to contribute to the clinical phenotype more fully explained by the primary neuropathological diagnosis. The contributing neuropathological diagnoses may also explain additional clinical features of the patient which cannot otherwise be attributed to the primary neuropathological diagnosis. "Incidental" neuropathological diagnoses are defined as coexistent neuropathological entities that are thought to contribute little, if at all, to the clinical presentation of the patient.

eReferences

1 ADNI. ADNI2 Procedures manual. . **94**, doi:doi:10.1002/ejoc.201200111.

2 Iaccarino, L. *et al.* Spatial Relationships between Molecular Pathology and Neurodegeneration in the Alzheimer's Disease Continuum. *Cerebral cortex (New York, N.Y. : 1991)* **31**, 1-14, doi:10.1093/cercor/bhaa184 (2021).

3 Baker, S. L., Maass, A. & Jagust, W. J. Considerations and code for partial volume correcting [18F]-AV-1451 tau PET data. *Data in brief* **15**, 648-657 (2017).

4 Lesman-Segev, O. H. *et al.* Diagnostic Accuracy of Amyloid versus (18) F-Fluorodeoxyglucose Positron Emission Tomography in Autopsy-Confirmed Dementia. *Ann Neurol* **89**, 389-401, doi:10.1002/ana.25968 (2021).

5 Lesman-Segev, O. H. *et al.* Tau PET and multimodal brain imaging in patients at risk for chronic traumatic encephalopathy. *NeuroImage. Clinical* **24**, 102025, doi:10.1016/j.nicl.2019.102025 (2019).

6 Klunk, W. E. *et al.* The Centiloid Project: standardizing quantitative amyloid plaque estimation by PET. *Alzheimer's & dementia : the journal of the Alzheimer's Association* **11**, 1-15.e11-14, doi:10.1016/j.jalz.2014.07.003 (2015).

7 Maass, A. *et al.* Comparison of multiple tau-PET measures as biomarkers in aging and Alzheimer's disease. *Neuroimage* **157**, 448-463, doi:10.1016/j.neuroimage.2017.05.058 (2017).